JCTC Journal of Chemical Theory and Computation

Article

pubs.acs.org/JCTC

Relaxation Mechanisms of 5-Azacytosine

Angelo Giussani,*[,†] Manuela Merchán,[†] João Paulo Gobbo,[‡] and Antonio Carlos Borin*[,‡]

[†]Instituto de Ciencia Molecular, Universitat de València, P.O. Box 22085, ES-46071 Valencia, Spain

[‡]Instituto de Química, Departamento de Química Fundamental, NAP-PhotoTech the USP Consortium for Photochemical Technology, Universidade de São Paulo, Avenida Professor Lineu Prestes 748, 05508-000 São Paulo, Brazil

Supporting Information

ABSTRACT: The photophysics and deactivation pathways of the noncanonical 5-azacytosine nucleobase were studied using the CASPT2//CASSCF protocol. One of the most significant differences with respect to the parent molecule cytosine is the presence of a dark $^1(n_N\pi^*)$ excited state placed energetically below the bright excited state $^1(\pi\pi^*)$ at the Franck−Condon region. The main photoresponse of the system is a presumably efficient radiationless decay back to the original ground state, mediated by two accessible conical intersections involving a population transfer from the $^1(\pi\pi^*)$ and the $^1(n_N\pi^*)$ states to the ground state. Therefore, a minor contribution of the triplet states in the photophysics of the system is expected, despite the presence of a deactivation path leading to the lowest $^3(\pi\pi^*)$ triplet state. The global scenario on the photophysics and photochemistry of the 5-azacytosine system gathered on theoretical grounds is consistent with the available experimental data, taking especially into account the low values of the singlet−triplet intersystem crossing and fluorescence quantum yields observed.

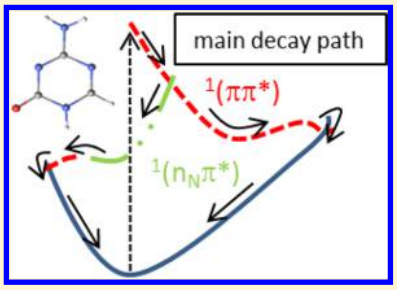

1. INTRODUCTION

The photostability of the five canonical nucleobases after ultraviolet (UV) absorption constitutes one of the most remarkable characteristics of these nucleobases. Nucleosides excited states produced by 263 nm radiation decay to the ground state in an ultrafast radiationless process in the range of 290−720 fs.[1] The lack of strong solvent effects and the similar photostability of the nucleosides and nucleotides suggests an intrinsic molecular property. They are extremely stable to photochemical events triggered by sunlight radiation, because they relax to the ground state before the excited states can react. Such short excited-state lifetimes suggest the existence of ultrafast decay channels, via internal conversion (IC) mechanisms, allowing the nonradiative release of the exceeding energy.

Ultrafast radiationless mechanisms involved in IC and intersystem crossing (ISC) are mediated by conical intersections (CIs) and singlet−triplet crossing (STC) regions.[2,3] To guarantee an efficient ultrafast relaxation process, the CIs and STC regions should become accessible along the main decay path.[2,4−9] In other words, a proper understanding of the photodecay mechanisms implies the location and mapping of the most relevant structures.

Cytosine is one of the five canonical nucleobases, with excited state lifetime within 1−3 ps[10] upon excitation from 260 (4.77 eV) to 290 nm (4.27 eV). The deactivation mechanisms have been the subject of a large set of theoretical work, employing the reaction path approach[11] (static approach) and nonadiabatic dynamics simulations with[12,13] and without[14−20] inclusion of spin−orbit coupling effects. The results point out to a complex sequence of events that can be collected in three distinct pathways, leading to two subpicosecond time scale features related to three different CIs. The coexistence of tautomeric forms in the gas phase brings further complexity to fully unveil the ultrafast excited-state dynamics of cytosine.[10,13,20−22]

Analogous nucleobases not found in DNA and RNA exhibit distinct photochemical properties.[4,23−27] For instance, 2-aminopurine has a strong emission enabling its use as a fluorescent probe for detecting conformational changes in proteins, while adenine (6-aminopurine)[4] has a very efficient quenching mechanism, resulting in a fluorescence quantum yields of about 10^{-4} in aqueous solution. Another example comes from 6-azauracil (6-AU) and uracil;[25,28,29] while uracil exhibits an ultrafast radiationless mechanism to the ground state via a CI, the process is not favorable in 6-AU because a relatively high energy barrier has to be surmounted. Regarding the population of the lowest triplet state, uracil and 6-AU exhibit similar mechanisms, although their efficiency is much more pronounced in 6-AU, for which high quantum yield of singlet−triplet intersystem crossing (ϕ_{ISC}) is observed, leading to O_2 ($^1\Delta_g$) (singlet oxygen) production in acetonitrile solution.

Cytosine and its derivatives are also a clear example of the dependence of the excited state lifetimes on the chemical structure. Starting with cytosine, Malone et al.[30] demonstrated that the $^1(L_a\ \pi\pi^*)$ (S_1) lifetime depends strongly on substitution of the C_5 atom. For example, the $^1(L_a\ \pi\pi^*)$ state of cytosine has a lifetime of about 1−3 ps, whereas substitution of C_5 hydrogen atom by a methyl group (5-methylcytosine: m^5Cyt) increases the S_1 lifetime to 7.2 ps; with a fluorine atom

Received: April 14, 2014
Published: August 11, 2014

   dx.doi.org/10.1021/ct5003175 | J. Chem. Theory Comput. 2014, 10, 3915−3924

replacing the C_5 hydrogen atom (5-fluorcytosine: fl^{5}Cyt), the S_1 lifetime increases to 88 ps, and if a N^{4}acetyl is the substituted group (N^4-acetylcytosine: ac^{4}Cyt) there is an even larger increase of the S_1 lifetime to 280 ps. Therefore, a chemical modification of the C_5 may disfavor the efficient and fast deactivation mechanism observed in cytosine, resulting in a species more prone for photochemical reactions.[31]

5-Azacytosine (5-AC, Figure 1), is a non-natural analogue of cytosine, on which the C_5 ring atom is substituted by a nitrogen

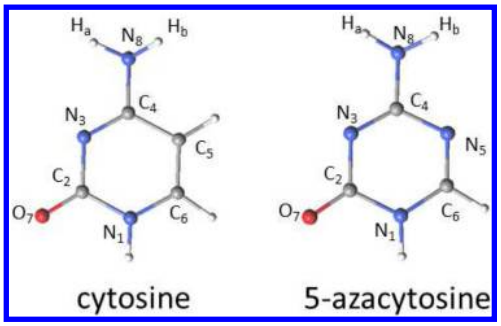

Figure 1. Numbering scheme for 5-azacytosine.

atom, resulting in the 1,3,5-triazinering. When attached to a ribose ring (5-azacytidine, also known as azacitidine), it constitutes an important chemotherapeutic agent;[32] in the presence of methyltransferases, it is incorporated into DNA during replication and into RNA during the transcription step, acting as an inhibitor of methyltransferases.[33,34] Upon excitation at 248 nm at room temperature,[26] 5-AC exhibits a very low ($<10^{-3}$) fluorescence quantum yield (ϕ_F), suggesting a fast deactivation mechanism as that observed in cytosine.

Although 5-AC has figured prominently in different therapies,[32] very little is known about its nonadiabatic photochemistry. Kobayashi et al.[26] have recently studied the excited states properties of 5-AC experimentally, by means of absorption, transient-absorption, and time-resolved thermal lensing. Time-dependent density functional theory (TDDFT) calculations were also carried out to aid the interpretation of the experimental results. The authors concluded that 5-AC has a very low ϕ_F and that the two lowest-lying singlet excited states (S_1 and S_2) are of $\pi\pi^*$ nature.

In this contribution, the excited states relaxation mechanisms in 5-AC were analyzed with the CASPT2//CASSCF protocol, which has been employed to compute state minima, STC regions, and CIs. Relaxations paths connecting the relevant structures were characterized by means of the minimum energy path (MEP) approach on the most important electronic hypersurfaces. The results lead to a comprehensive relaxation scheme both in the singlet and triplet manifold.

2. METHODOLOGY

The present study was performed by using the well-tested CASPT2//CASSCF methodology[35−39] as implemented in the MOLCAS 7.6 software.[40] Optimized structures and MEPs were calculated at the multiconfigurational CASSCF level. At the geometries so obtained, dynamic correlation effects were taken into account by performing second-order multiconfigurational CASPT2 calculations. All computations were carried out by imposing no symmetry restrictions to the molecule (C_1 symmetry). Basis sets of atomic natural orbital (ANO) of L-type contracted to C,N,O[3s,2p,1d]/H[2s1p] were employed (ANO-L double-ζ plus polarization).[41]

The employed active space comprises a total of 14 electrons distributed among 10 orbitals, CASSCF(14,10) (Figure 2), obtained as following. The full valence active space of cytosine,

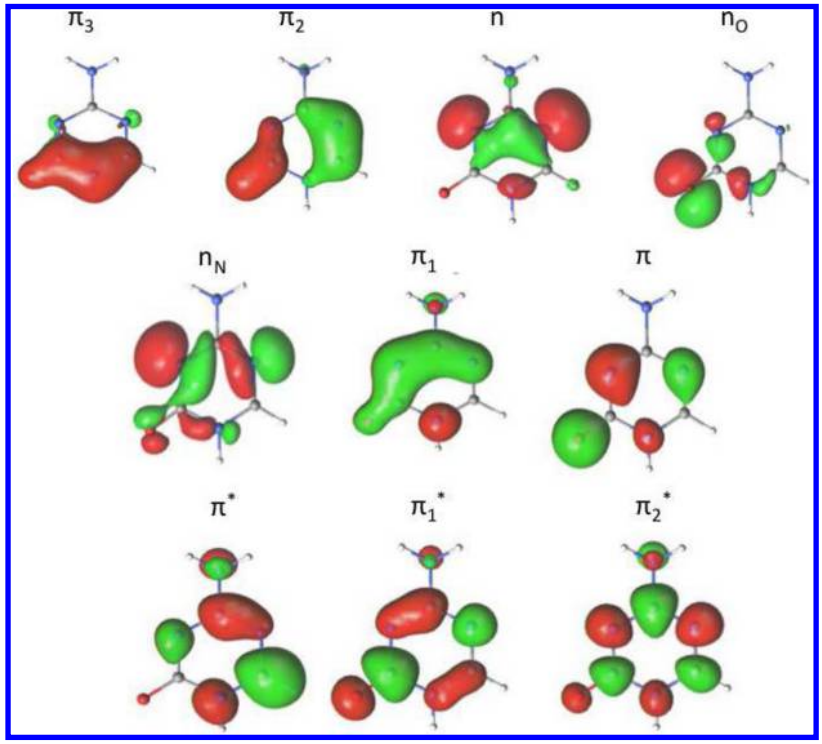

Figure 2. Active space in terms of averaged valence natural orbitals computed at the CASSCF level (CAS(14,10)/ANO-L double-ζ plus polarization level), in the ground-state equilibrium geometry.

dx.doi.org/10.1021/ct5003175 | J. Chem. Theory Comput. 2014, 10, 3915−3924

the natural analogue of 5-AC, consists of eight π orbitals and two lone pairs (one on O_7 and the other on N_3 atoms), resulting in 14 active electrons distributed among 10 active orbitals (CAS(14,10)). Previous studies have shown that the use of a reduced CAS(12,9) active space, in which the π orbital localized on the amino group is not present, provides a correct description of the low-lying electronic states of cytosine.[12,42] In the present work on 5-AC, the analogue CAS(12,9) active space of cytosine was used, expanded by the inclusion of the lone pair localized on the new nitrogen atom, N_5. The employed active space is then formed by 14 active electrons distributed among 10 active orbitals (CAS(14,10)), seven have π character, and three describe lone pairs (Figure 2). After test calculations (Supporting Information, Tables S1−S3), the final CASSCF wave functions for both the singlet and triplet manifold were obtained through a state-averaged procedure over four roots with equal weights. The obtained CASSCF energies were corrected performing single-state CASPT2 calculations. For the CASPT2 calculations, an imaginary level-shift correction of 0.2 au was used to minimize the effects of possible intruder states.[43] The standard CASPT2 zeroth-order Hamiltonian was employed as originally implemented.[36] The core orbitals were frozen in the CASPT2 calculations. Such a CASPT2 approach has been validated during the last decades in many different studies of organic molecules, providing a correct prediction, description, and interpretation of photophysical and photochemical experimental data.[9,29,44−48]

MEPs were computed at the CASSCF level of theory as steepest descent paths.[49] CIs and STCs searches were performed using the restricted Lagrange multipliers technique;[49] in this approach, the lowest-energy point is obtained under the restriction of degeneracy between the two considered states. A structure is here considered as a CI and/or a STC region if two electronic states having the same or different spin multiplicity, respectively, present an energy gap at the CASPT2 level not larger than ∼0.1 eV. To search for such geometries, the strategy here employed and already used in other studies,[47,48] consists in performing single-point CASPT2 calculations along the path obtained by means of a CASSCF CI optimization. This approach takes advantage of the fact that, in the neighborhood of a CASSCF degenerate structure, a CASPT2 degenerate point has been in many cases found, as for example in references 47 and 48. Spin−orbit coupling (SOC) elements were computed within the AMFI (atomic mean field integrals), as was done in previous works.[29,45,46] Where specified, solvent effects were taken into account with the polarized continuum model (PCM).[50] Cartesian coordinates for relevant structures can be found in the Supporting Information.

3. RESULTS AND DISCUSSION

3.1. Franck−Condon Geometry. The optimized geometrical parameter for the ground-state equilibrium structure of 5-AC, $^1(gs)_{min}$, are shown in Figure 3 and Table 1. In comparison to the ground state geometry of cytosine,[42,51,52] the replacement of the C_5 atom by a nitrogen atom (N_5) shortens the C_4-N_5 (1.397 Å) and N_5-C_6 (1.279 Å) bond distances, while the N_1-C_2 (1.403 Å) bond becomes longer. As compared to cytosine, the bond angles $N_3-C_4-N_5$ (126.8°), $N_5-C_6-N_1$ (123.4°), and $H-N_8-H$ (115.7°) in the amino group become larger, while the $C_4-N_5-C_6$ (114.3°) bond angle is somewhat smaller. The resulting optimized parameters

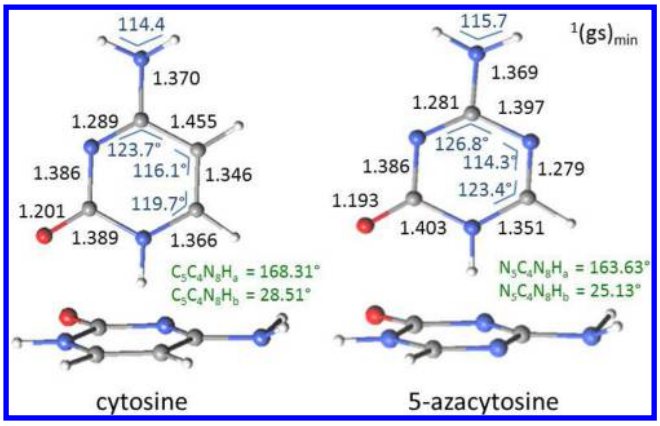

Figure 3. Frontal and side views of 5-azacytosine CASSCF ground state minima structure, $^1(gs)_{min}$, including selected bond lengths (in Å) and bond angles (in degrees). For the sake of comparison, the ground state optimized structure of cytosine from a previous study[42] is also displayed.

for 5-AC are in agreement with those reported by Podolyan et al.[51]

The computed spectroscopic properties for the low-lying singlet and triplet electronic states of 5-AC are listed in Table 2, along with other selected theoretical results and related experimental values. In the present work, attention was focused on the lowest-lying excited states (S_1, S_2, T_1, and T_2), due to their relevance from the photophysical and photochemical standpoints.

The absorption spectrum of 5-AC has been recorded by Kobayashi et al.[26] in acetonitrile (aprotic and polar solvent), which has two broad absorption bands centered, respectively, at 4.77 eV (260 nm) and 5.51 eV (225 nm), showing the latter the strongest intensity. For cytosine there is a larger number of experimental spectra available. Clark et al.[53] reported an absorption band at about 4.5 eV (277 nm) in trimethyl phosphate solution, while the band is centered in the vapor phase[54] around 4.77 eV (260 nm). Abouaf et al.[55] have recently reported an experimental gas-phase vertical excitation energy of 4.65 ± 0.1 eV. Absorption spectra[56−58] in water revealed a low energy band centered between 4.56 and 4.65 eV.

Theoretical studies[11] indicate that the lowest-lying singlet electronic states of cytosine are, in order of increasing energy, of $\pi\pi^*$, $n_O\pi^*$, and $n_N\pi^*$ character, with the S_1 $^1(\pi\pi^*)$ the bright state. The $^3(\pi\pi^*)$ state is the lowest excited state, placed at 3.53 eV above the ground state at the Franck−Condon (FC) region.

According to our results (Table 2), this pattern is not observed in 5-AC, for which the lowest singlet excited state is of $^1(n_N\pi^*)$ nature, characterized by a CASSCF wave function basically described by a singly excited configuration from an n orbital mainly localized on the nitrogen atoms (n_N orbital, Figure 2) to the π^* molecular orbital (Figure 2 and Supporting Information, Figure S1). The electronic transition to the S_2 $^1(\pi\pi^*)$ excited state is predicted to carry most of the intensity upon UV irradiation. The S_2 $^1(\pi\pi^*)$ CASSCF wave function is mainly composed by the $\pi \rightarrow \pi^*$ one-electron promotion (Supporting Information, Figure S2).

The T_1 $^3(\pi\pi^*)$ and T_2 $^3(n_N\pi^*)$ excited states are located below the S_1 $^1(n_N\pi^*)$ and S_2 $^1(\pi\pi^*)$ singlet excited states. The T_1 $^3(\pi\pi^*)$ excited state, described mainly by a $\pi \rightarrow \pi^*$ one-electron promotion similar to the one characterizing the S_2 $^1(\pi\pi^*)$ state (Supporting Information, Figure S2), is placed

dx.doi.org/10.1021/ct5003175 | J. Chem. Theory Comput. 2014, 10, 3915−3924

Table 1. Optimized Geometrical Parameters of 5-Azacytosine

	ground state			this work		
bond length[a]	this work	ref 26	ref 51	$S_1\ ^1(n_N\pi^*)$	$S_2\ ^1(\pi\pi^*)$	$T_1\ ^3(\pi\pi^*)$
N_1-C_2	1.403	1.417	1.429	1.409	1.361	1.382
C_2-N_3	1.386	1.362	1.375	1.382	1.280	1.389
N_3-C_4	1.281	1.333	1.318	1.349	1.413	1.404
C_4-N_5	1.397	1.385	1.392	1.291	1.280	1.283
N_5-C_6	1.279	1.304	1.302	1.396	1.390	1.398
C_6-N_1	1.351	1.346	1.348	1.406	1.389	1.398
C_2-O_7	1.193	1.230	1.222	1.190	1.320	1.210
C_4-N_8	1.369	1.340	1.350	1.370	1.375	1.382
bond angle[b]						
$N_1-C_2-N_3$	115.0	115.9	114.5	112.1	124.1	117.5
$C_2-N_3-C_4$	119.0	118.3	118.3	126.7	113.9	115.8
$N_3-C_4-N_5$	126.8	126.7	128.4	117.4	126.1	124.4
$C_4-N_5-C_6$	114.3	114.1	112.9	118.9	116.8	117.3
$N_5-C_6-N_1$	123.4	123.5	123.5	114.5	116.9	116.9
$C_6-N_1-C_2$	121.4	121.4	122.4	115.3	117.4	120.0
$N_3-C_4-N_8$	120.1		118.3	118.9	112.7	113.4
$C_4-N_8-H_a$	115.2	119.9	118.3	114.1	113.9	113.5
$C_4-N_8-H_b$	115.1	120.0	118.8	112.9	114.1	113.0
$H_a-N_8-H_b$	115.7	120.1	120.6	113.2	114.3	112.9
$N_1-C_2-O_7$	120.6	119.8	118.9	123.3	113.6	123.2
C_2-N_1-H	117.6	120.7	116.1	112.2	118.6	116.2
$N5-C_6-H$	119.9	119.8	119.5	117.0	118.7	116.5

[a]Bond distances in angstroms. [b]Bond angles in degrees.

Table 2. Singlet and Triplet Low-Lying Electronic States of 5-Azacytosine

	gas phase—this work[a]					acetonitrile						
	absorption[b]			emission[c]		this work[a]			TDDFT[26]			exp[26]
state[d]	E_v^{abs}	f^e	μ^f	E_v^{emi}	T_e^g	state[d]	E_v^{abs}	f	state	E_v^{abs}	f	λ_{max}^h
S_0	0.00		4.26			S_0	0.00		S_0	0.00		
$T_1\ ^3(\pi\pi^*)$	4.33		1.89	2.20	3.27	$T_1\ ^3(\pi\pi^*)$	4.40		$T_1\ ^3(\pi\pi^*)$	4.03		
$T_2\ ^3(n_N\pi^*)$	4.38		2.44			$T_2\ ^3(n_N\pi^*)$	4.52		$T_2\ ^3(n_N\pi^*)$	4.12		
$S_1\ ^1(n_N\pi^*)$	4.46	0.008	2.54	2.08	3.59	$T_3\ ^3(\pi\pi^*)$	4.67		$T_3\ ^3(\pi\pi^*,n_N\pi^*)$	4.35		
$S_2\ ^1(\pi\pi^*)$	4.74	0.062	3.54	2.30	3.69	$S_1\ ^1(n_N\pi^*)$	4.69	0.010	$S_1\ ^1(\pi\pi^*)$	4.66	0.003	
$T_3\ ^3(\pi\pi^*)$	5.13		2.89			$S_2\ ^1(\pi\pi^*)$	4.80	0.077	$T_4\ ^3(n\pi^*)$	4.79		
$T_4\ ^3(n_O\pi^*)$	5.57		3.00			$T_4\ ^3(n_O\pi^*)$	4.82		$S_2\ ^1(\pi\pi^*)$	5.00	0.014	4.77
$S_3\ ^1(n_O\pi^*)$	5.58	0.002	2.89			$S_3\ ^1(n_O\pi^*)$	5.06	0.000	$S_3\ ^1(n\pi^*)$	5.23	0.001	
						$T_5\ ^3(\pi\pi^*)$	5.27		$S_4\ ^1(\pi\pi^*,n\pi^*)$	5.34	0.076	5.51
						$T_6\ ^3(\pi\pi^*)$	5.28					
						$S_4\ ^1(\pi\pi^*)$	5.51	0.031				

[a]*This work* refers to values obtained at the CASPT2//CASSCF(14,10)/ANO-L double-ζ plus polarization level of theory simulating, when required, acetonitrile solvent using the PCM model. [b]Vertical absorption excitation energy (E_v^{abs}, eV). [c]Vertical emission excitation energy (E_v^{emi}, eV). [d]The labels indicate states of similar natures. [e]Oscillator strengths (f). [f]Dipole moments (μ, Debye). [g]Band origin (T_e, eV). [h]Experimental maximum absorption energy (λ_{max}, eV). λ_{max} = 260 nm, $S_2\ ^1(\pi\pi^*)$ state and 225 nm, $S_4\ ^1(\pi\pi^*,n\pi^*)$ state.

vertically 4.33 eV above the ground state. On the other hand, the $T_2\ ^3(n_N\pi^*)$ state, vertically computed to be at 4.38 eV above the ground state, has $n_N \rightarrow \pi^*$ character, with a CASSCF wave function characterized by the $n_N \rightarrow \pi^*$ singly excited configuration (Figure 2 and Supporting Information, Figure S1).

Therefore, according to our CASPT2//CASSCF results, the order of the states in the low energetic region is (vertical excitation energies within parentheses): $T_1\ ^3(\pi\pi^*)$ (4.33 eV) < $T_2\ ^3(n_N\pi^*)$ (4.38 eV) < $S_1\ ^1(n_N\pi^*)$ (4.46 eV) < $S_2\ ^1(\pi\pi^*)$ (4.74 eV). The same energetic ordering was obtained irrespective of the number of states computed (Supporting Information, Tables S1−S3).

As expected, replacing cytosine C_5 ring atom by nitrogen causes a large perturbation on the $n\pi^*$ and $\pi\pi^*$ excited states. On the basis of the results presented above, this chemical modification stabilizes the $^3(\pi\pi^*)$ and $^3(n_N\pi^*)$ states by 0.80 and 0.56 eV, respectively, making then the lowest excited states in 5-AC and destabilizes the $^1(\pi\pi^*)$, which is blue-shifted by 0.33 eV. Regarding the lowest $^1(n\pi^*)$ state, in 5-AC it is localized on the nitrogen atoms ($^1(n_N\pi^*)$), while in cytosine it is localized on the oxygen atom ($^1(n_O\pi^*)$). Furthermore, the lowest 5-AC $^1(n\pi^*)$ state is red-shifted by 0.28 eV, while in cytosine it is shift to the blue by 0.53 eV with respect to the lowest $^1(\pi\pi^*)$ state.

The T_3, T_4, and S_3 excited states of 5-AC were also computed and the corresponding data are reported in Table 2.

dx.doi.org/10.1021/ct5003175 | J. Chem. Theory Comput. 2014, 10, 3915−3924

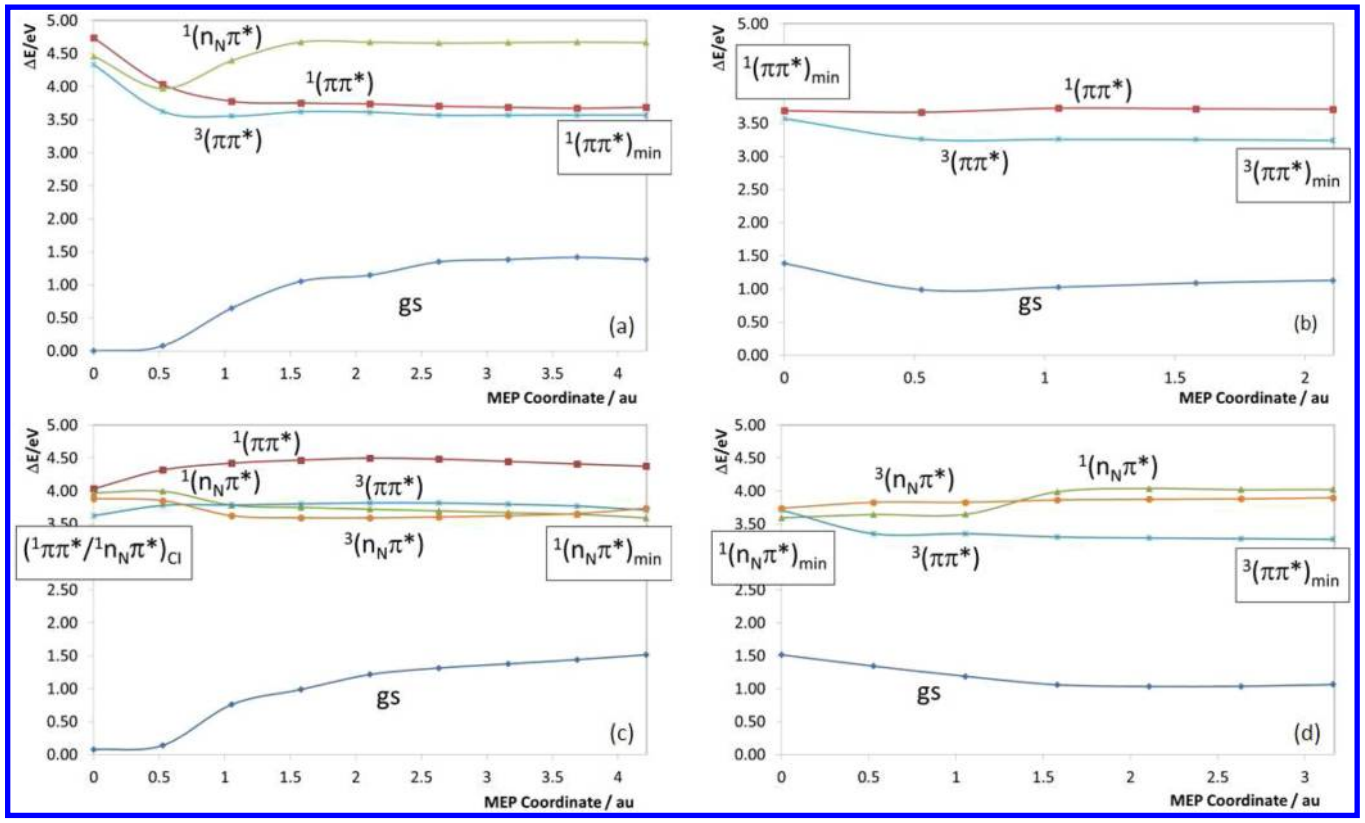

Figure 4. Energy profiles of the ground and lowest singlet and triplet excited states of 5-azacytosine along the minimum energy path (MEP) computed at the CASPT2//CASSCF(14,10)/ANO-L double-ζ plus polarization level: (a) $^1(\pi\pi^*)$ MEP from the Franck−Condon geometry ($^1(gs)_{min}$); (b) $^3(\pi\pi^*)$ MEP from the $^1(\pi\pi^*)_{min}$ structure; (c) $^1(n_N\pi^*)$ MEP from $(^1\pi\pi^*/^1n_N\pi^*)_{CI}$ conical intersection; and (d) $^3(\pi\pi^*)$ MEP from the $^1(n_N\pi^*)_{min}$ geometry.

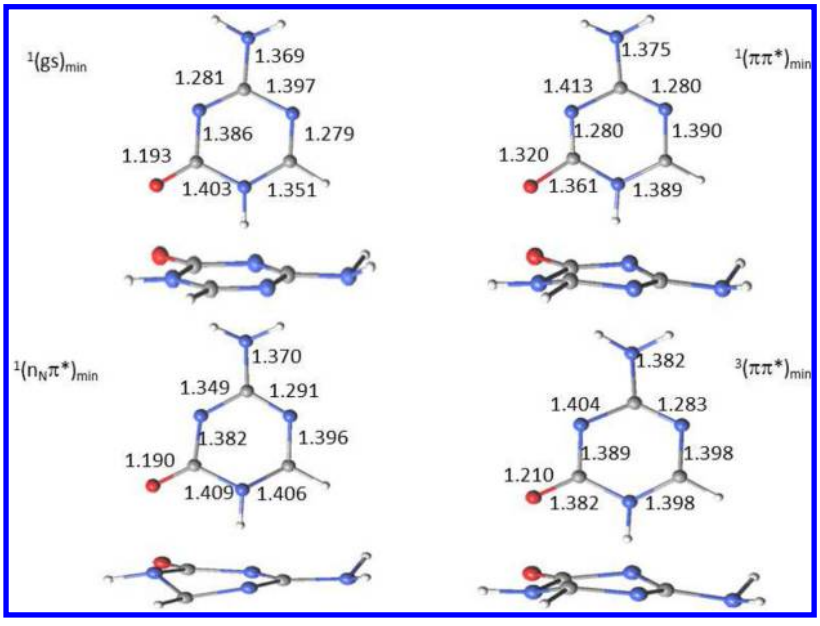

Figure 5. Frontal and side views of 5-azacytosine CASSCF minima structures including selected bond lengths (in Å).

The T_3 state displays $\pi\pi^*$ nature (Supporting Information, Figure S3), while T_4 and S_3 are both mainly described by a one-electron promotion from the lone pair mainly localized on the O_7 atom (the n_O orbital) to the π^* orbital (Supporting Information, Figure S4).

Since the T_3 $^3(\pi\pi^*)$ state never appears to be involved in the studied photochemical and photophysical processes, in the following the $^3(\pi\pi^*)$ label indicates the triplet electronic state having a CASSCF wave function basically described by a singly excited configuration among the orbitals π and π^* (Supporting Information, Figure S2).

To get a better comparison with the experimental results in acetonitrile,[26] vertical calculations at the FC geometry were performed using the PCM model to simulate solvent effects,

dx.doi.org/10.1021/ct5003175 | J. Chem. Theory Comput. 2014, 10, 3915−3924

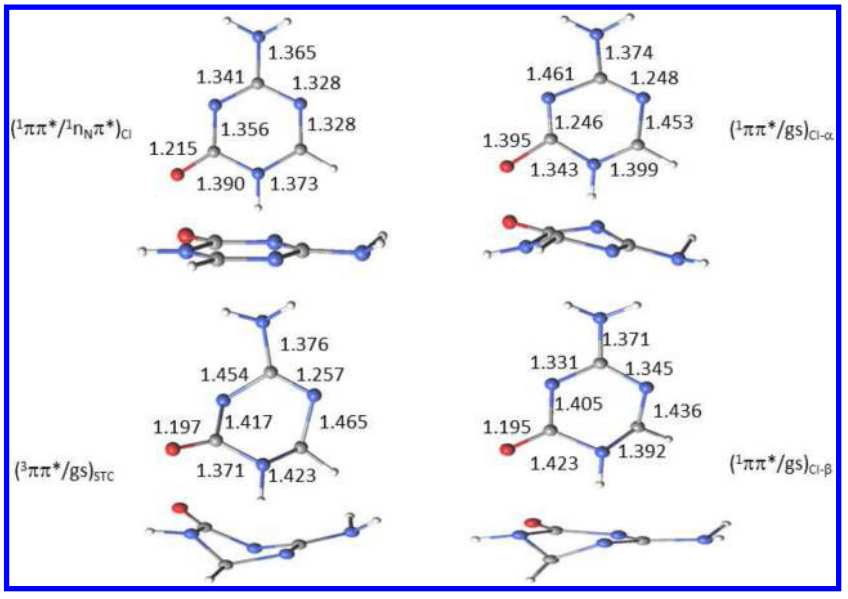

Figure 6. Frontal and side views of 5-azacytosine CASPT2 degenerate structures (see Methodology; either conical intersection or intersystem crossing region). Selected bond lengths (in Å) are also shown.

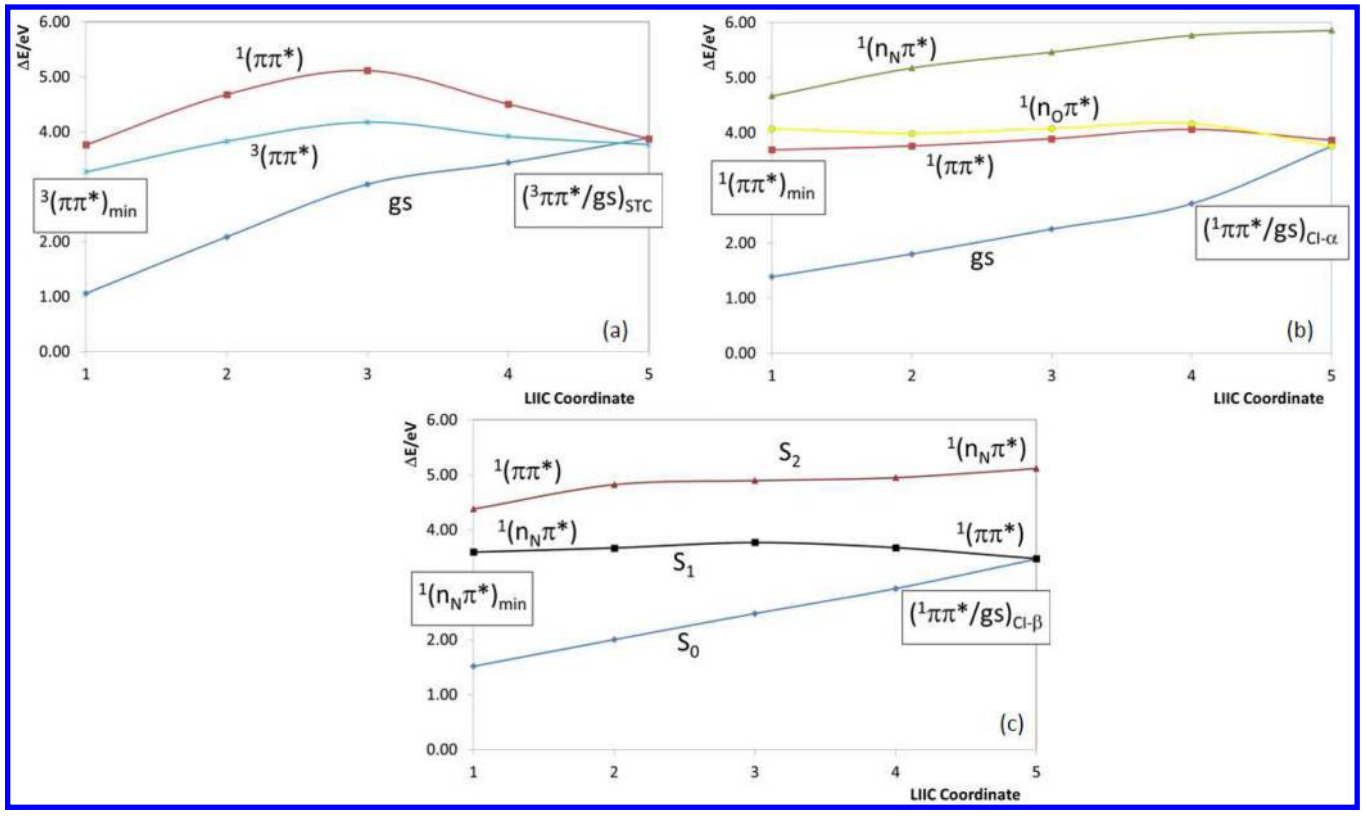

Figure 7. Energy profiles of the ground and lowest singlet and triplet excited states of 5-azacytosine along the linear interpolations of internal coordinates (LIIC) profiles computed at the CASPT2//CASSCF(14,10) ANO-L double-ζ plus polarization level: (a) LIIC between the $^3(\pi\pi^*)_{min}$ and the $(^3\pi\pi^*/gs)_{STC}$ structures; (b) LIIC between the $^1(\pi\pi^*)_{min}$ and the $(^1\pi\pi^*/gs)_{CI-\alpha}$ structures; and (c) LIIC between the $^1(n_N\pi^*)_{min}$ and the $(^1\pi\pi^*/gs)_{CI-\beta}$ geometries.

employing the nonequilibrium approach for several excited states. The reaction field was generated for the lowest singlet excited state, and seven singlet and triplet electronic states were computed. The results are reported in Table 2, together with previous theoretical outcomes and experimental data. Comparing the CASPT2 vertical absorption excitation energies with the one calculated at the time-dependent density functional theory level by Kobayashi et al.,[26] it is possible to find some similarities, as well as differences. The three lowest triplet excited states (T_1, T_2, and T_3) have the same energy order and similar natures at both levels of theory. The three low-lying singlet excited states have, however, a different nature and order: at the CASPT2 level the S_1 state has $n\pi^*$ nature, the S_2 presents $\pi\pi^*$ character, and the S_3 displays an $n \rightarrow \pi^*$

dx.doi.org/10.1021/ct5003175 | J. Chem. Theory Comput. 2014, 10, 3915−3924

excitation, while at the TDDFT both S_1 and S_2 have $\pi\pi^*$ character, and the S_3 presents $n\pi^*$ nature. Regarding the comparison with the experimental data, it seems plausible to relate the experimental absorption band centered at 4.77 eV (260 nm) to the computed S_2 $^1(\pi\pi^*)$ state, while the strongest band observed experimentally at 5.51 eV (225 nm) can be assigned to the computed S_4 $^1(\pi\pi^*)$ state in acetonitrile. The latter is mainly described by a single $\pi \rightarrow \pi^*$ excitation (Supporting Information, Figure S5), and it was computed in vacuum as the S_6 $^1(\pi\pi^*)$ state (Supporting Information, Table S2) at higher energy, 6.25 eV. It is possible to appreciate that almost the same energetic order characterizes both the gas phase and acetonitrile situations, with the only exception constituted by the T_3 $^1(\pi\pi^*)$ state position, lower in acetonitrile than in vacuum.

3.2. Deactivation Pathways. On the basis of the computed oscillator strengths (Table 2) the bright excited state of 5-AC corresponds to the $^1(\pi\pi^*)$ state, from which consequently the most important photophysical events are expected to take place. As displayed in Figure 4a, the MEP along the $^1(\pi\pi^*)$ excited state evolves barrierless from the FC geometry to an equilibrium structure, $^1(\pi\pi^*)_{min}$, placed adiabatically 3.69 eV above the ground-state minimum. In comparison to the FC geometry, the most striking geometrical distortions observed along the computed MEP involve a single−double bond inversion and a slight pyramidalization of the C_6 atom (Figure 5). A similar structural deformation is also observed along the MEP for the bright state $^1(\pi\pi^*)$ of cytosine.[42,59]

Another interesting feature, observed at the beginning of the computed MEP on the $^1(\pi\pi^*)$ excited state, is the existence of a CI between the $^1(\pi\pi^*)$ and the $^1(n_N\pi^*)$ states, hereafter denoted as $(^1\pi\pi^*/^1n_N\pi^*)_{CI}$ (Figure 6). Therefore, the MEP along the $^1(\pi\pi^*)$ hypersurface starting at the FC region reveals that the system can reach the $^1(\pi\pi^*)_{min}$ structure and the $^1(n_N\pi^*)$ dark state through the $(^1\pi\pi^*/^1n_N\pi^*)_{CI}$ CI. The MEP on the $^1(n_N\pi^*)$ hypersurface from the $(^1\pi\pi^*/^1n_N\pi^*)_{CI}$ structure evolves to a minimum geometry, $^1(n_N\pi^*)_{min}$, located 3.59 eV adiabatically above the FC region (Figures 4c and 5).

In comparison to the FC geometry, the $(^1\pi\pi^*/^1n_N\pi^*)_{CI}$ structure shows an elongation of the C_3-C_4 (Δd = 0.06 Å), C_5-C_6 (Δd = 0.05 Å), C_1-C_6 (Δd = 0.02 Å), and C_2-O_7 (Δd = 0.02 Å) bond lengths, while the C_1-C_2 (Δd = −0.01 Å), C_2-C_3 (Δd = −0.03 Å), C_4-N_8 (Δd = −0.03 Å), and C_4-C_5 (Δd = −0.07 Å) are decreased.

The $^1(\pi\pi^*)_{min}$ and $^1(n_N\pi^*)_{min}$ optimized structures represent STC regions. In fact, the lowest singlet excited state, either the $^1(\pi\pi^*)$ or the $^1(n_N\pi^*)$ state at the $^1(\pi\pi^*)_{min}$ and $^1(n_N\pi^*)_{min}$ regions, respectively, is almost degenerate with the lowest triplet $^3(\pi\pi^*)$ state, displaying an energy gap of about 0.12 eV (2.8 kcal·mol^{-1}). The computed SOC are equal to 11.8 and 17.1 cm^{-1} at the respective $^1(\pi\pi^*)_{min}$ and $^1(n_N\pi^*)_{min}$ geometries. The $^1(\pi\pi^*)_{min}$ and $^1(n_N\pi^*)_{min}$ structures will then be also named as $(^1\pi\pi^*/^3\pi\pi^*)_{STC}$ and $(^1n_N\pi^*/^3\pi\pi^*)_{STC}$. In both situations the lowest triplet state can decay to an equilibrium region, $^3(\pi\pi^*)_{min}$, placed 3.27 eV above the minimum of the ground state (Figure 4b,d). An STC region between the $^3(\pi\pi^*)$ and the ground state, hereafter indicated as $(^3\pi\pi^*/gs)_{STC}$, was found 0.62 eV above the $^3(\pi\pi^*)_{min}$ optimized geometry. Since the computed energy barrier connecting such geometries obtained by a linear interpolation of internal coordinates (LIIC) calculation is equal to 0.91 eV (Figure 7a and Supporting Information, Table S6), it is reasonable to assume that the $(^3\pi\pi^*/gs)_{STC}$ plays a minor role on the decay experimented by the excited 5-AC.

Despite the possibility to populate the triplet states, the system can from both the $^1(\pi\pi^*)_{min}$ and $^1(n_N\pi^*)_{min}$ minimum structures decay back to the original ground state through a nonradiative process mediated by the presence of a nearby CI. A CI involving the $^1(\pi\pi^*)$ and the ground state, hereafter $(^1\pi\pi^*/gs)_{CI-\alpha}$, was located slightly above the $^1(\pi\pi^*)_{min}$ (Table 3 and Figure 6). A closer comparison between the $^1(\pi\pi^*)_{min}$ and $(^1\pi\pi^*/gs)_{CI-\alpha}$ structures indicates a great similarity between them, with both exhibiting the key geometrical distortion found in the so-called cytosine bond-inversion CI.[11] The 5-AC $(^1\pi\pi^*/gs)_{CI-\alpha}$ can then be coined as a bond-inversion CI. A LIIC calculation (Figure 7b), which provides an upper bond to the path connecting two regions of the potential energy hypersurface,[47,48] reveals that the $^1(\pi\pi^*)_{min}$ and $(^1\pi\pi^*/gs)_{CI-\alpha}$ structures are linked by an energy barrier of 0.37 eV (Supporting Information, Table S7). It is then possible to assume that the system will may decay from the $^1(\pi\pi^*)_{min}$ geometry to the original ground state through the $(^1\pi\pi^*/gs)_{CI-\alpha}$ CI. The process will be particularly favored when an excess of energy is provided.

The $(^1\pi\pi^*/gs)_{CI-\alpha}$ structure actually constitutes a three-state CI, since both the $^1(\pi\pi^*)$ state and the $^1(n_O\pi^*)$ state are degenerate in energy with the ground state (Table 3). Such a situation was also described for the cytosine system by Blancafort and Robb,[60] and is consequently probably related to the nature of the distortion that characterizes the bond-inversion CI in both the 5-AC and cytosine molecules.

Starting from the $^1(n_N\pi^*)_{min}$ optimized structure (that is, on a region where the $^1(n_N\pi^*)$ state becomes the lowest singlet excited state), the search of a degenerate structure between the lowest singlet excited and the ground state ended up with the $^1(\pi\pi^*/gs)_{CI-\beta}$ CI (Figure 6). Such a degenerate region can be regarded as an ethene-like CI, since it is characterized by a localized distortion on the N_5-C_6 double bond, similar to the one found in the CI described in the ethene molecule.[61]

At the $(^1\pi\pi^*/gs)_{CI-\beta}$ region, the lowest singlet excited state that is degenerated with the ground state is the $^1(\pi\pi^*)$. The computation of a LIIC calculation (Figure 7c) between the $^1(n_N\pi^*)_{min}$ and the $(^1\pi\pi^*/gs)_{CI-\beta}$ structures has shown that such a change in the nature of the lowest singlet excited states occurs presumably without any crossing between the $^1(\pi\pi^*)$ and the $^1(n_N\pi^*)$ states. Along the computed LIIC path connecting the $^1(n_N\pi^*)_{min}$ structure to the $(^1\pi\pi^*/gs)_{CI-\beta}$ CI a small energy barrier of 0.18 eV was obtained on the S1

Table 3. Computed Energies (eV) for the Most Relevant Singlet and Triplet States of 5-Azacytosine at Different Important Geometries

	state[a]				
structure	gs	$^1(\pi\pi^*)$	$^1(n_N\pi^*)$	$^1(n_O\pi^*)$	$^3(\pi\pi^*)$
$^1(\pi\pi^*)_{min}$	1.39	3.69	4.67	4.08	3.57
$^1(n_N\pi^*)_{min}$	1.52	4.38	3.59		3.71
$^3(\pi\pi^*)_{min}$	1.06	3.76	4.02	4.65	3.27
$(^1\pi\pi^*/^1n_N\pi^*)_{CI}$	0.08	4.04	3.97	4.80	3.63
$(^1\pi\pi^*/gs)_{CI-\alpha}$	3.75	3.87		3.76	4.27
$(^1\pi\pi^*/gs)_{CI-\beta}$	3.47	3.47	5.12		3.89
$(^1\pi\pi^*/^3\pi\pi^*)_{STC}$	3.89	3.87			3.77

[a]All the reported values are referred to the ground state optimized geometry, $^1(gs)_{min}$.

dx.doi.org/10.1021/ct5003175 | J. Chem. Theory Comput. 2014, 10, 3915−3924

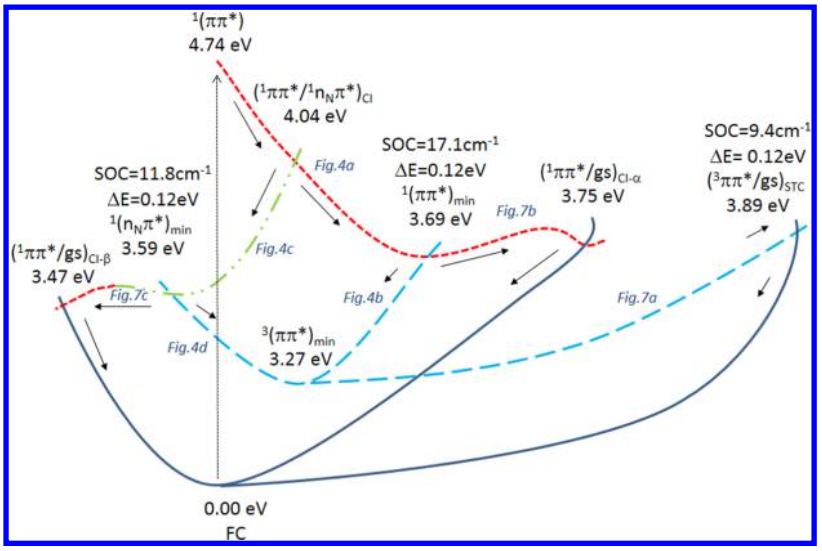

Figure 8. Schematic representation of the 5-AC deactivation pathways. Dashed red, dash-dot-dot-dash green, dashed pale blue, and solid blue lines indicate the evolution of the system on the $^1(\pi\pi^*)$, $^1(n_N\pi^*)$, $^3(\pi\pi^*)$, and ground state, respectively, obtained via the computed CASPT2//CASSCF minimum energy path and linear interpolation of internal coordinates. The italic labels, close to each line, indicate the number of original figure describing the corresponding path. All the reported results are based on CASPT2 energies.

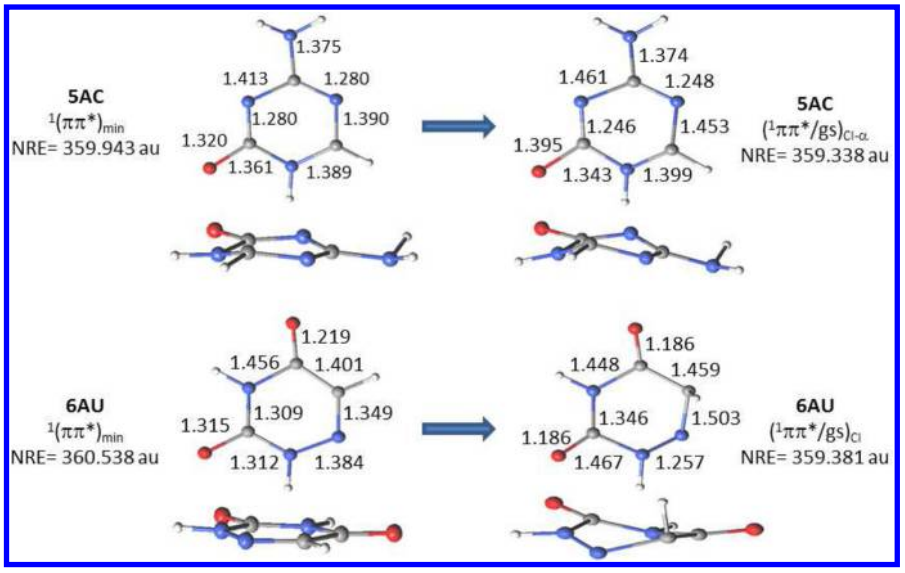

Figure 9. Frontal and side views of the $^1(\pi\pi^*)$ minimum structure and the corresponding conical intersection with the ground state for 5-azacytosine (5-AC) and 6-azauracil (6-AU). The nuclear repulsion energies (NRE) of the different geometries and selected bond lengths (in Å) are also reported.

potential energy hypersurface (Supporting Information, Table S8). Because of such a low energy barrier, the system can efficiently evolve through the $(^1\pi\pi^*/gs)_{CI-\beta}$ CI back to the original ground state structure.

An important photophysical aspect of 5-AC refers to its low quantum yield of singlet−triplet intersystem crossing, preventing its application to obtain O_2 $(^1\Delta_g)$. As it is related to population transfer to the triplet-state, it is worth evaluating this possibility with the described relaxation mechanisms.

According to our results, the $^1(\pi\pi^*)_{min}$ and $^1(n_N\pi^*)_{min}$ structures are prone for triplet-state population, via ISC mechanisms to the $^3(\pi\pi^*)$ state. Nonetheless, as described above, presumably more efficient IC pathways mediated by the $(^1\pi\pi^*/gs)_{CI-\alpha}$ and the $(^1\pi\pi^*/gs)_{CI-\beta}$ CIs take place in the same regions. Therefore, the IC decays are more likely to occur than the population of the triplet-state via ISC, diminishing the quantum yield of singlet−triplet intersystem crossing and, consequently, the possibility of employing 5-AC in a O_2 $(^1\Delta_g)$ formation process, for which very high quantum yield of singlet−triplet intersystem crossing are mandatory. This conclusion is in line with the experimental data obtained in acetonitrile by Kobayashi et al.,[26] who reported a very low quantum yield of singlet−triplet intersystem crossing after excitation with a 248 nm (5.0 eV) radiation. This energy is in fact sufficient to populate the bright state $^1(\pi\pi^*)$ from which IC decays, via the $(^1\pi\pi^*/gs)_{CI-\alpha}$ and the $(^1\pi\pi^*/gs)_{CI-\beta}$ CIs, can take place. The decay paths characterized in this work at the CASPT2//CASSCF, and described previously, probably constitute the main relaxation mechanisms of 5AC, and are summarized in Figure 8.

dx.doi.org/10.1021/ct5003175 | J. Chem. Theory Comput. 2014, 10, 3915−3924

3.3. Comparison with 6-Azauracil. Having described the deactivation mechanisms of 5-AC, a comparison with the related system 6-AU is at this point appropriate.

6-AU is another non-natural modified nucleobases, resulting from the substitution by a nitrogen atom of the C6 carbon of an uracil molecule. It has been studied by Kobayashi et al.[26] by means of different experimental techniques and from a theoretical standpoint by Gobbo at al.,[29] using the CASPT2//CASSCF protocol. Unlike 5-AC, 6-AU has a high quantum yield of singlet−triplet intersystem crossing (Φ_{ISC} = 1.00 ± 0.10). Such property can be ascribed to an efficient population mechanism of the T_1 $^3(\pi\pi^*)$ state, which can be summarized in two steps. First, the bright $^1(\pi\pi^*)$ state of the system evolves barrierless to a minimum region, where the $^1(n_O\pi^*)$ and the $^3(n_O\pi^*)$ can be populated by means of the $(^1n_O\pi^*/^1\pi\pi^*)_{CI}$ CI and the $(^3n_O\pi^*/^1\pi\pi^*)_{STC}$ STC region, respectively. Second, the presence of the $(^1n_O\pi^*/^3\pi\pi^*)_{STC}$ STC region and the $(^3n_O\pi^*/^3\pi\pi^*)_{CI}$ CI ultimately lead to the population of the $^3(\pi\pi^*)$ state. In particular, the path mediated by the $(^1n_O\pi^*/^3\pi\pi^*)_{STC}$ singlet−triplet crossing region can be considered very efficient due to the high computed SOC, equal to 64,7 cm^{-1}, and the zero-energy gap between the involved states.

For 5-AC, the $^1(n_N\pi^*)_{min}$ and the $^1(\pi\pi^*)_{min}$ are both STC regions, but the corresponding ISC processes are probably not as much efficient as the one mediated by the $(^1n_O\pi^*/^3\pi\pi^*)_{STC}$ geometry observed in 6-AU. First, the energy gaps that characterized such degenerate regions are much larger (0.12 eV) and the computed SOC are considerable smaller (11.8 and 17.1 cm^{-1}, respectively). Second, from both the $^1(n_N\pi^*)_{min}$ and the $^1(\pi\pi^*)_{min}$ structures the decay to the triplet manifold is in direct competition with an efficient radiationless decay process via the $(^1\pi\pi^*/gs)_{CI-\alpha}$ and $(^1\pi\pi^*/gs)_{CI-\beta}$ CIs, respectively.

Actually in the 6-AU system a nonradiative decay from the minimum of the $^1(\pi\pi^*)$ state has also been obtained, mediated by an accessible CI named as $(^1\pi\pi^*/gs)_{CI}$.[29] In comparison with the decay path described in 5-AC from the $^1(\pi\pi^*)$ state minimum to the $(^1\pi\pi^*/gs)_{CI-\alpha}$ region, the radiationless process found in 6-AU is less favorable since a larger energy barrier of 0.55 eV, against 0.37 eV in 5-AU, needed to be surmounted. Besides, there is a closer geometrical resemblance between the $^1(\pi\pi^*)$ state minimum and the $(^1\pi\pi^*/gs)_{CI-\alpha}$ CI in 5-AC than between the $^1(\pi\pi^*)_{min}$ structure and the $(^1\pi\pi^*/gs)_{CI}$ CI in 6-AU (Figure 9).

Kobayashi et al.[26] considered that the photophysical behavior of 6-AU and 5-AC differs in acetonitrile because in the former the $^1(n\pi^*)$ state is placed below the bright excited $^1(\pi\pi^*)$ state at the FC region, favoring a further state switch to the $^3(\pi\pi^*)$ state, while for 5-AC, the $^1(n\pi^*)$ state at the FC region is above the bright state, preventing an efficient population of the $^1(n\pi^*)$ state and, consequently, of the $^3(\pi\pi^*)$ state. On the basis of our gas-phase results, for 5-AC the $^1(n\pi^*)$ state is lower in energy than the $^1(\pi\pi^*)$ state at the FC region and can be populated. The key for not observing a population transfer to the $^3(\pi\pi^*)$ state is probably due to the presence of a more efficient state switch to the ground state via the described CIs.

4. CONCLUSIONS

The photophysics of 5-azacytosine has been studied with the CASPT2//CASSCF protocol in conjunction with ANO-L double-ζ plus polarization basis sets. According to our results, the photophysics of 5-azacytosine is characterized by a fast and radiationless decay back to the ground state. Starting at the Franck−Condon region, the initially populated bright $^1(\pi\pi^*)$ excited state can either evolve to the $^1(\pi\pi^*)_{min}$ minimum, or decay thought the $(^1\pi\pi^*/^1n_N\pi^*)_{CI}$ conical intersection to the minimum of the $^1(n_N\pi^*)$ state, $^1(n_N\pi^*)_{min}$. From both the $^1(\pi\pi^*)_{min}$ and $^1(n_N\pi^*)_{min}$ regions, it has been shown that the system can evolve to a nearby conical intersection with the ground state ($(^1\pi\pi^*/gs)_{CI-\alpha}$ and $(^1\pi\pi^*/gs)_{CI-\beta}$, respectively), after surmounting a relative small energy barrier (0.37 and 0.18 eV, respectively). Such conditions consequently determine the photostability of the system, in agreement with the low values of the quantum yield of singlet−triplet intersystem crossing and of the fluorescence quantum yield experimentally reported. Despite that a partial population transfer to the lowest $^3(\pi\pi^*)$ triplet state is possible, the process can be considered of minor relevance since it is in direct competition with the most efficient radiationless decay mediated by the $(^1\pi\pi^*/gs)_{CI-\alpha}$ and $(^1\pi\pi^*/gs)_{CI-\beta}$ conical intersections.

■ ASSOCIATED CONTENT

Supporting Information

Tabulated data indicating calculated vertical excitation and other energies, illustrations indicating orbitals mainly involved in, for example, the $^{1,3}(n_N\pi^*)$ and $^{1,3}(\pi\pi^*)$ states, among others, and Cartesian coordinates for the stationary points. This material is available free of charge via the Internet at http://pubs.acs.org/.

■ AUTHOR INFORMATION

Corresponding Authors

*E-mail: ancborin@iq.usp.br. (A.C.B.)
*E-mail: Angelo.Giussani@uv.es. (A.G.)

Notes

The authors declare no competing financial interest.

■ ACKNOWLEDGMENTS

J.P.G. thanks FAPESP (Fundação de Amparo à Pesquisa do Estado de São Paulo) for financial support. A.C.B. thanks continuous academic support from the CNPq (Conselho Nacional de Desenvolvimento Científico e Tecnológico) and the Laboratory of Advanced Scientific Computation (LCCA) of the Univ. of São Paulo. The authors thank the support by Project CTQ2010-14892 of the Spanish MEC/FEDER. A.G. gratefully acknowledges a Ph.D. fellowship "V segles" from the Universitat de València.

■ REFERENCES

(1) Crespo-Hernández, C. E.; Cohen, B.; Hare, P. M.; Kohler, B. *Chem. Rev.* **2004**, *104*, 1977−2020.
(2) Olivucci, M. In *Computational Photochemistry;* Olivucci, M., Ed.; Elsevier: Amsterdam, 2005.
(3) *Conical Intersections;* Domcke, W., Yarkony, D. R., Eds.; World Scientific: Singapore, 2004.
(4) Serrano-Andrés, L.; Merchán, M.; Borin, A. C. *Proc. Natl. Acad. Sci. U.S.A.* **2006**, *103*, 8691−8696.
(5) Serrano-Andrés, L.; Merchán, M.; Borin, A. C. *Chem.—Eur. J.* **2006**, *12*, 6559−6571.
(6) Kistler, K. A.; Matsika, S. *J. Phys. Chem. A* **2007**, *111*, 2650−2661.
(7) Zgierski, M. Z.; Patchkovskii, S.; Lim, E. C. *Can. J. Chem.* **2007**, *85*, 124−134.
(8) Serrano-Andrés, L.; Merchán, M.; Borin, A. C. *J. Am. Chem. Soc.* **2008**, *130*, 2473−2484.
(9) Serrano-Andrés, L.; Merchán, M. Chapter 16. In *Radiation Induced Molecular Phenomena in Nucleic Acid: A Comprehensive*

Theoretical and Experimental Analysis; Shukla, M., Leszczynski, J., Eds.; Springer: Berlin, 2008; Vol. *5*, pp 435 − 472.
(10) Kosma, K.; Schröter, C.; Samoylova, E.; Hertel, I. V.; Schultz, T. *J. Am. Chem. Soc.* **2009**, *131*, 16939−16943.
(11) Giussani, A.; Segarra-Martí, J.; Roca-Sanjuán, D.; Merchán, M. Excitation of Nucleobases from a Computational Perspective I: Reaction Paths. *Top. Curr. Chem.* **2013**, DOI: 10.1007/128_2013_501.
(12) Richter, M.; Marquetand, P.; González-Vázquez, J.; Sola, I.; González, L. *J. Phys. Chem. Lett.* **2012**, *3*, 3090−3095.
(13) Sebastian, M.; Marquetand, P.; Martin, R.; González-Vázquez, J.; González, L. *ChemPhysChem* **2013**, *14*, 2920−2931.
(14) Barbatti, M.; Aquino, A. J. A.; Szymczak, J. J.; Nachtigallová, D.; Hobza, P.; Lischka, H. *Proc. Natl. Acad. Sci. U.S.A.* **2010**, *107*, 21453−21458.
(15) Barbatti, M.; Aquino, A. J. A.; Szymczak, J. J.; Nachtigallová, D.; Lischka, H. *Phys. Chem. Chem. Phys.* **2011**, *13*, 6145−6155.
(16) Hudock, H. R.; Martínez, T. J. *ChemPhysChem* **2008**, *9*, 2486−2490.
(17) Markwick, P. R. L.; Doltsinis, N. L. *J. Chem. Phys.* **2007**, *126*, 175102.
(18) Zhenggang, L.; Fabiano, E.; Thiel, W. *J. Phys. Chem. B* **2009**, *113*, 3548−3555.
(19) González-Vázquez, J.; González, L. *ChemPhysChem* **2010**, *11*, 3617−3624.
(20) Nakayama, A.; Harabuchi, Y.; Yamazaki, S.; Taketsugu, T. *Phys. Chem. Chem. Phys.* **2013**, *15*, 12322−12339.
(21) Ulrich, S.; Schultz, T.; Stolow, M. Z. Z. A. *Phys. Chem. Chem. Phys.* **2004**, *6*, 2796−2801.
(22) Ho, J.; Yen, H.; Chou, W.; Weng, C.; Cheng, L.; Shi, H.; Lai, S.; Cheng, P. *J. Phys. Chem. A* **2011**, *115*, 8406−8418.
(23) Canuel, C.; Mons, M.; Pluzzi, F.; Tardivel, B.; Dimicoli, I.; Elhanine, M. *J. Chem. Phys.* **2005**, *122*, 074316.
(24) Blancafort, L.; Cohen, B.; Hare, P. M.; Robb, M. A. *J. Phys. Chem. A* **2005**, *109*, 4431−4436.
(25) Kobayashi, T.; Harada, Y.; Suzuki, T.; Ichimura, T. *J. Phys. Chem. A* **2008**, *112*, 13308−13315.
(26) Kobayashi, T.; Kuramochi, H.; Harada, Y.; Suzuki, T.; Ichimura, T. *J. Phys. Chem. A* **2009**, *113*, 12088−12093.
(27) Harada, Y.; Okabe, C.; Kobayashi, T.; Suzuki, T.; Ichimura, T.; Nishi, N.; Xu, Y. *J. Phys. Chem. Lett.* **2010**, *1*, 480−484.
(28) Etinski, M.; Marian, C. *Phys. Chem. Chem. Phys.* **2010**, *12*, 15665−15671.
(29) Gobbo, J. P.; Borin, A. C.; Serrano-Andrés, L. *J. Phys. Chem. B* **2011**, *115*, 6243−6251.
(30) Malone, R. J.; Miller, A. M.; Kohler, B. *Photochem. Photobiol.* **2003**, *77*, 158−164.
(31) Tommasi, S.; Denissenko, M. F.; Pfeifer, G. P. *Cancer Res.* **1997**, *57*, 4727−4730.
(32) Lubbert, M. *Curr. Top. Microbiol. Immunol.* **2000**, *249*, 135−164.
(33) Santi, D. V.; Garret, C. E.; Barr, P. J. *Cell* **1983**, *33*, 9−10.
(34) Jones, P. A. *Cell* **1985**, *40*, 485−486.
(35) Roos, B. O. In *Advances in Chemical Physics; Ab Initio Methods in Quantum Chemistry - II;* Lawley, K. P., Ed.; John Wiley & Sons Ltd.: Chichester, England, 1987; Vol. *69*, pp 399.
(36) Andersson, K.; Malmqvist, P.-Å.; Roos, B. O. *J. Chem. Phys.* **1992**, *96*, 1218−1226.
(37) Roos, B. O.; Andersson, K.; Fülscher, M. P.; Malmqvist, P.-Å.; Serrano-Andrés, L.; Pierloot, K.; Merchán, M. In *Advances in Chemical Physics: New Methods in Computational Quantum Mechanics;* Prigogine, I., Rice, S. A., Eds.; Wiley: New York, 1996; Vol. *93*, pp 219.
(38) Merchán, M.; Serrano-Andrés, L.; Fülscher, M. P.; Roos, B. O. In *Recent Advances in Multireference Methods;* Hirao, K., Ed.; World Scientific Publishing Company: Amsterdam, 1999; Vol. *4*, pp 161.
(39) Merchán, M.; Serrano-Andrés, L. Ab Initio Methods for Excited States. In *Computational Photochemistry;* Olivucci, M., Ed.; Elsevier: Amsterdam, 2005; p 35.
(40) Aquilante, F.; De Vico, L.; Ferré, N.; Ghigo, G.; Malmqvist, P.-Å.; Pedersen, T.; Pitonak, M.; Reiher, M.; Roos, B. O.; Serrano-Andrés, L.; Urban, M.; Veryazov, V.; Lindh, R. *J. Comput. Chem.* **2010**, *31*, 224−247.
(41) Widmark, P.-O.; Malmqvist, P.-Å.; Roos, B. O. *Theor. Chem. Acc.* **1990**, *77*, 291−306.
(42) Merchán, M.; Serrano-Andrés, L. *J. Am. Chem. Soc.* **2003**, *125*, 8108−8109.
(43) Forsberg, N.; Malmqvist, P.-Å. *Chem. Phys. Lett.* **1997**, *274*, 196−204.
(44) Serrano-Andrés, L.; Merchán, M. *J. Photochem. Photobiol., C* **2009**, *10*, 21−32.
(45) Gobbo, J. P.; Borin, A. C. *J. Phys. Chem. B* **2012**, *116*, 14000−14007.
(46) Gobbo, J. P.; Borin, A. C. *J. Phys. Chem. A* **2013**, *117*, 5589−5596.
(47) Giussani, A.; Merchán, M.; Roca-Sanjuán, D.; Lindh, R. *J. Chem. Theory Comput.* **2011**, *7*, 4088−4096.
(48) Giussani, A.; Serrano-Andrés, L.; Merchán, M.; Roca-Sanjuán, D.; Garavelli, M. *J. Phys. Chem. B* **2013**, *117*, 1999−2004.
(49) De Vico, L.; Olivucci, M.; Lindh, R. *J. Chem. Theory Comput.* **2005**, *1*, 1029−1037.
(50) Barone, V.; Improta, R.; Rega, N. *Acc. Chem. Res.* **2008**, *41*, 605−616.
(51) Podolyan, Y.; Rubin, Y. R.; Leszczynski, J. *J. Phys. Chem. A* **2000**, *104*, 9964−9970.
(52) Tomic, K.; Tatchen, J.; Marian, C. M. *J. Phys. Chem. A* **2005**, *109*, 8410−8418.
(53) Clark, L. B.; Tinoco, I. *J. Am. Chem. Soc.* **1965**, *87*, 11−15.
(54) Clark, L. B.; Peschel, G. G.; Tinoco, I. *J. Phys. Chem.* **1965**, *69*, 3615−3618.
(55) Abouaf, R.; Pommier, J.; Dunet, H.; Quan, P.; Nam, P.; Nguyen, M. T. *J. Chem. Phys.* **2004**, *121*, 11668.
(56) Voelter, W.; Records, R.; Bunnenberg, E.; Djerassi, C. *J. Am. Chem. Soc.* **1968**, *90*, 6163−6163.
(57) Du, H.; Fuh, R. C. A.; Li, J. Z.; Corkan, L. A.; Lindsey, J. S. *Photochem. Photobiol.* **1998**, *68*, 141−142.
(58) Middleton, C. T.; de La Harpe, K.; Su, C.; Law, Y. K.; Crespo-Hernández, C. E.; Kohler, B. *Annu. Rev. Phys. Chem.* **2009**, *60*, 217−239.
(59) Ismail, N.; Blancafort, L.; Olivucci, M.; Kohler, B.; Robb, M. A. *J. Am. Chem. Soc.* **2002**, *124*, 6818−6819.
(60) Blancafort, L.; Robb, M. *J. Phys. Chem. A* **2004**, *108*, 10609−10614.
(61) Barbatti, M.; Paier, J.; Lischka, H. *J. Chem. Phys.* **2004**, *121*, 11614.